2015

Image processing methods for in situ estimation of cohesive sediment floc size, settling velocity, and density

SJ Smith

Carl T. Friedrichs
Virginia Institute of Marine Science

LIMNOLOGY
and
OCEANOGRAPHY: METHODS

ASLO

Limnol. Oceanogr.: Methods 13, 2015, 250–264

doi: 10.1002/lom3.10022

Image processing methods for in situ estimation of cohesive sediment floc size, settling velocity, and density

S. Jarrell Smith,*[1] Carl T. Friedrichs[2]

[1]U.S. Army Engineer Research and Development Center, Coastal and Hydraulics Laboratory, Vicksburg, Mississippi, USA
[2]Virginia Institute of Marine Science, The College of William and Mary, Gloucester Point, Virginia, USA

Abstract

Recent advances in development of in situ video settling columns have significantly contributed toward fine-sediment dynamics research through concurrent measurement of suspended sediment floc size distributions and settling velocities, which together also allow inference of floc density. Along with image resolution and sizing, two additional challenges in video analysis from these devices are the automated tracking of settling particles and accounting for fluid motions within the settling column. A combination of particle tracking velocimetry (PTV) and particle image velocimetry (PIV) image analysis techniques is described, which permits general automation of image analysis collected from video settling columns. In the fixed image plane, large-particle velocities are determined by PTV and small-particle velocities are tracked by PIV and treated as surrogates for fluid velocities. The large-particle settling velocity (relative to the suspending fluid) is determined by the vector difference of the large and small-particle settling velocities. The combined PTV/PIV image analysis approach is demonstrated for video settling column data collected within a dredge plume in Boston Harbor. The automated PTV/PIV approach significantly reduces uncertainties in measured settling velocity and inferred floc density.

Fine grained sediments in riverine, estuarine, and marine environments form flocs composed of organic and inorganic material (Eisma 1986; Van Leussen 1994; Ayukai and Wolanski 1997; Williams et al. 2008). Flocs formed in suspension vary in size, shape, and density dependent on factors such as mineralogy, organic coatings, internal shear, and sediment concentration (Eisma 1986; Tsai et al. 1987; Ayukai and Wolanski 1997; Manning and Dyer 1999). The larger size of flocs results in settling velocities several orders of magnitude faster than the constituent particles (Van Leussen and Cornelisse 1993). Additionally, the size, shape, density, and settling velocity of flocs are time-variable as influenced by time- and space-variant hydrodynamics and suspended sediment populations (Eisma 1986; Van der Lee 2000). Fine sediments are of key interest in estuarine and marine systems through the influence of light attenuation, delivery of sediment and nutrients to the sediment bed, and geomorphology of estuaries, river deltas, and continental shelves (Van Leussen 1994; Ayukai and Wolanski 1997; Hill et al. 2000; Sanford et al. 2005). Fine-sediment dynamics are also important factors in engineering studies of navigation and dredging, contaminant transport, and ecosystem restoration (Tsai et al. 1987; Mehta 1989; Santschi et al. 2005; Smith and Friedrichs 2011).

The fragile nature of flocs requires in situ sampling to accurately characterize their properties under field conditions (Gibbs and Konwar 1983; Van Leussen and Cornelisse 1993; Fennessy et al. 1994; Dyer et al. 1996). In situ settling velocities have been obtained by gravimetric analysis (Owen 1976; Cornelisse 1996), optical methods (Kineke et al. 1989; Agrawal and Pottsmith 2000), acoustic-based Reynolds flux (Fugate and Friedrichs 2002; Voulgaris and Meyers 2004; Cartwright et al. 2013), or imaging (Van Leussen and Cornelisse 1993; Fennessy et al. 1994; Sternberg et al. 1996; Syvitski and Hutton 1996; Mikkelsen et al. 2004; Sanford et al. 2005; Smith and Friedrichs 2011). The imaging methods generally use an underwater video camera that images flocs settling within an enclosed settling column. One advantage of the imaging methods is that settling velocity and two-dimensional (2-D) size are collected concurrently for individual particles, permitting floc density estimates through application of Stokes settling or modifications of the drag relationship for higher Reynolds numbers (Oseen 1927; Schiller and Naumann 1933). Dyer et al. (1996) summarizes concerns with the in situ

*Correspondence: Jarrell.Smith@erdc.dren.mil

devices, which include: floc breakup during sample capture, flocculation by differential settling within the sampler, and fluid circulation within the imaging chamber.

Fluid motions within the settling column of in situ video devices arise from turbulence introduced during sample capture, thermally induced circulation, volume displacement of the settling particles, and motion of the settling column. Various approaches have been used to minimize and/or account for fluid motions within the settling columns of in situ video systems. Van Leussen and Cornelisse (1993) and Fennessy et al. (1994) use separate sample collection and settling chambers and additionally introduce density stratification within their settling chamber to damp turbulence introduced during sample collection. This approach has resulted in general success in their systems, but Van Leussen and Cornelisse (1993) and Fennessy et al. (1994) indicate that fluid motions are still apparent in some of their experiments. To address these fluid motions, Van Leussen and Cornelisse (1993) adjust the settling velocities of large particles with fluid motions estimated by manually tracking the smallest visible particles as a surrogate for fluid motions. The two-chamber approach has an additional advantage in that particles from the capture/stilling chamber settle into clear water, which permits settling velocity estimates in high suspended sediment concentrations that would otherwise be too turbid for image acquisition.

The two-chamber devices have a significant disadvantage associated with the long measurement period required to permit particles with small settling velocities to settle from the capture chamber to the imaging zone within the settling column. For applications that require rapid measurement, such as within dredge plumes or vertical profiling experiments, the 30–40 min measurement period limits vertical and temporal resolution of the measurements. Smith and Friedrichs (2011) developed the Particle Imaging Camera System (PICS) with a single capture and settling chamber and adopted the approach of Van Leussen and Cornelisse (1993), using the motions of the smallest visible particles as surrogates for fluid motion. Smith and Friedrichs determined the mean fluid motion from manually tracking 10 particles distributed in time and space within their image sequences. While this approach was considered better than neglecting the fluid motions, the manual tracking method is tedious, labor-intensive, and contributes a relatively large source of error in the settling velocity estimates (primarily from the time- and space-averaging of the fluid motions). An automated approach to quantifying fluid motions within the settling column, as suggested by Van Leussen and Cornelisse (1993), is sought to permit rapid sampling for a single-chamber video settling column with greatly reduced measurement error.

Particle tracking velocimetry (PTV) and particle image velocimetry (PIV) are two image analysis methods commonly used in fluid dynamics research. The PTV method involves tracking of individual particles, whereas PIV involves correlating motions of groups of particles. Image processing for cohesive sediment settling experiments has been predominantly confined to PTV methods, both manual (Van Leussen and Cornelisse 1993; Fennessy and Dyer 1996; Manning and Dyer 2002; Sanford et al. 2005) and automated (Lintern and Sills 2006; Smith and Friedrichs 2011). This article describes an automated image processing method using both PTV and PIV methods to determine cohesive sediment fall velocities from in situ video devices. Combined PTV and PIV methods have been utilized to separately track the velocities of solid vs. liquid (or gas) components in two-phase turbulent flows (Kiker and Pan 2000; Khalitov and Longmire 2002). However, this is the first automated application of this technique to the calculation of sediment fall velocity.

Materials and procedures

The image processing methods described here were developed for the PICS (Smith and Friedrichs 2011) but should be generally applicable to other similar systems. PICS consists of a single-chambered, 100-cm long, 5-cm inner diameter settling column which captures and images particle settling from a minimally disturbed suspended sediment sample. Following sample capture, turbulence within the column is allowed to dissipate ($\sim$ 15–30 s) and a 30-s image sequence is collected at approximately 10 fps. The imaged region within the settling column is approximately 14 mm wide, 10 mm high, and 1 mm deep (aperture limited) with resolution of 1360×1024 pixels. Image acquisition is accomplished with a monochrome Prosilica GE1380 Gigabit Ethernet camera, 25-mm Pentax c-mount lens, and 15 mm extension tube. Lighting is provided with two white light-emitting diode arrays which are collimated to a three-millimeter thick light sheet in the focal plane. Additional description of PICS image acquisition and system characteristics is provided by Smith and Friedrichs (2011).

Challenges in analyzing the image sequences from in situ video devices (such as PICS) include the large numbers of particles to track, the low relative abundance of large particles which may contain most of the suspended sediment mass (Eisma 1986; Van Leussen 1994; Manning and Dyer 2002; Smith and Friedrichs 2011), and fluid circulation within the settling column (Van Leussen 1994; Sanford et al. 2005). The low abundance but large sediment mass fraction of the larger macroflocs (diameter, $d > 150$ μm) requires either large sampling volumes, or long sampling records to obtain statistically significant results. This suggests that large numbers of particles should be tracked in the video sequences. Because manual tracking methods are very labor-intensive, automated image processing methods are well suited for this task.

Two image processing methods are presented that accomplish the tasks of individually tracking larger particles (for

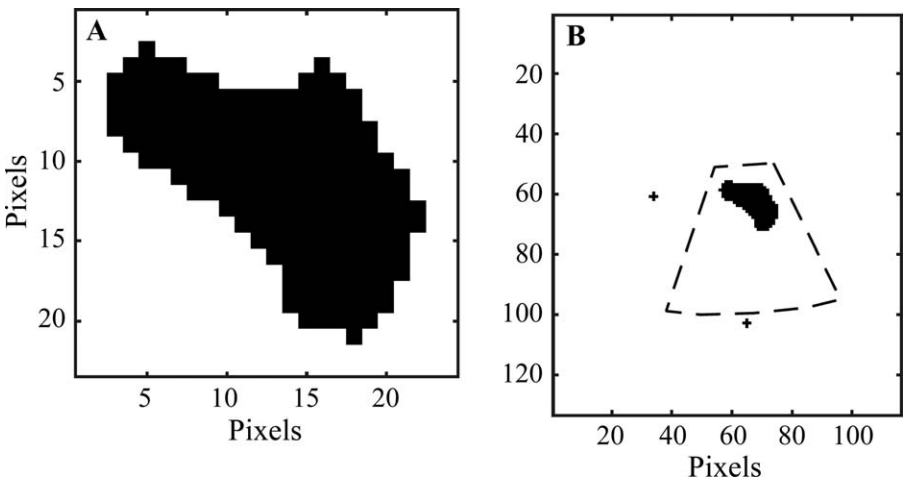

Fig. 1. Examples of (A) PTV kernel and (B) target image zones with initial (outer rectangle) and reduced search (dashed region) areas for cross-correlation peak.

settling velocity estimates) and tracking smaller particles for fluid velocity estimates. Large particles are defined here as particles large enough that their size may be determined with reasonable accuracy by image processing techniques. Several pixels are required to reliably determine particle size (Milligan and Hill 1998; Mikkelsen et al. 2004; Lintern and Sills 2006). The 3×3 pixel minimum of Mikkelsen et al. (2004) is selected for this application, resulting in a minimum resolvable particle size of approximately 30 μm. Small particles are defined as particles with sufficiently small mass and settling velocity such that their motions approximate that of the fluid in which they are suspended. (The criteria for PIV tracer particles are discussed later.) Details of the image analysis methods are provided in the next two sections; additional useful background on PIV and PTV methods are provided, e.g., in Adrian (1991), Raffel et al. (2007), and Steinbuck et al. (2010). All image processing routines described herein were programmed in Matlab, utilizing the Image Processing Toolbox.

Particle tracking velocimetry

Large particles ($d > 30$ μm) were tracked by PTV methods. The digital images were preconditioned prior to PTV, including background intensity leveling, grayscale to binary conversion, and digital erosion and dilation. First, spatial variations in illumination and imaging sensor noise were corrected by subtracting background image intensity. Background image intensity was determined as the modal (most frequently occurring) intensity for each pixel within a video sequence. The modal pixel intensity effectively identifies the background illumination by identifying the most consistent lighting level for each pixel (including ambient lighting and pixel noise). The background illumination field is determined for an entire image sequence and is subtracted from each image frame prior to additional processing.

Next, grayscale images are converted to binary using a grayscale thresholding method. By this method, pixels with intensities equal to or exceeding the globally applied threshold intensity are assigned logical true (1) and those with pixel intensity less than the threshold are assigned logical false (0). Determination of the grayscale threshold is somewhat subjective and is either prescribed by manual inspection for a representative set of image sequences or automatically by the method described by Lintern and Sills (2006). Following the conversion from grayscale to binary, holes within the defined particles are filled by binary dilation and erosion (Gonzalez et al 2004; Lintern and Sills 2006).

PTV is applied only to particles with equivalent spherical diameters greater than 30 μm. Here, we define equivalent diameter as $d = \sqrt{4A/\pi}$, where A is the 2-D, projected particle area after binary conversion. The 30-μm diameter criterion is consistent with that used by Milligan and Hill (1998) and Mikkelsen et al. (2004), and represents a reasonable lower limit of particle size resolution. Each binary particle meeting the size criterion is labeled and particle metrics are stored (such as centroid position, area, equivalent spherical diameter, major/minor axis lengths, and particle orientation).

The next step in the PTV method is to match particles between adjacent video frames. This is accomplished by comparing an image subset bounding a single particle (the kernel) in frame I to a larger subset of pixels (the target) in frame $I+1$. The initial target search area in frame $I+1$ is centered at the particle position in frame I and is set sufficiently large to ensure a particle match for the fastest settling particles, accounting for the time between images (vertical and horizontal extents of the target box are six times the particle length and three times the particle width, respectively). Example particle kernel and target interrogation areas are provided in Fig. 1.

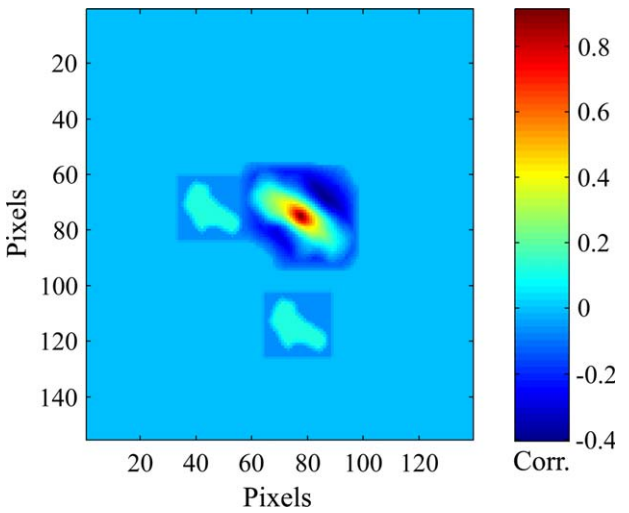

Fig. 2. Normalized cross-correlation matrix of kernel and target from Fig. 1.

The peak normalized cross-correlation (Haralick and Shapiro 1992; Lewis 1995) of the kernel and target interrogation areas defines the best match between the single particle in frame I to potential matches within the target area in frame $I+1$. The normalized cross-correlation matrix for the kernel and target from Fig. 1 is presented in Fig. 2. The location of maximum correlation is evaluated to determine if a valid particle exists at that location and whether its size and shape match that of the kernel particle within acceptable limits. For this example, the normalized correlation threshold is 0.6, the size criterion permits up to 25% change in particle area, and the shape criterion permits up to 15% change in the ratio of the minor-to-major particle dimensions. If all these criteria are met, then the kernel particle and target particles are labeled as matching, and forward and backward references (by particle and frame indices) are associated with the matched particles.

Once a successful match is determined, the velocity at frame $I+1$ is determined from the particle centroid displacement and frame interval, $\boldsymbol{V} = \Delta\boldsymbol{X}/\Delta t$, where $\boldsymbol{V}$ is the velocity vector, $\boldsymbol{X}$ is particle centroid position vector, and t is time. $\Delta\boldsymbol{X}$ is determined from the PTV particle centroid displacement, not the cross-correlation displacement, so the estimate has subpixel accuracy. Particles settling in the column are observed to nearly exclusively settle in stable orientations, with very little rotation or tumbling. So this is not expected to impact the centroid displacements significantly. The velocity history of a particle is then used to develop a smaller target interrogation area as shown in Fig. 1, which reduces the computational requirements and frequency of false matches. Note that this is similar to but not quite the same as some existing hybrid PIV/PTV approaches for velocimetry. For example, Cowen and Monismith (1997), use their previous time step PIV (i.e., fluid velocity) calculations to constrain PTV interrogation areas, whereas the present approach here uses the previous PTV (i.e., large-particle velocity) calculations for this purpose. The Cowen and Monismith (1997) method would not work here because of polydisperse suspension conditions, for which the settling velocity varies strongly among the particles.

On cycling through an entire video sequence, each frame includes labeled binary particles with information regarding the matched particles in adjacent frames. From this mapping of particle matches, sequences of matched particles following through all frames may be constructed. The ensemble of matches for a single particle across all possible frames is referred to here as a thread. A thread includes descriptive data (such as size, shape, location, velocity) about the single particle as it progresses from frame-to-frame in the image sequence. The collection of threads provides the basis for determining relationships between particle size, shape, and settling velocity.

Particle image velocimetry

Particle velocities determined by the PTV method are relative to the fixed reference frame of the image (or camera). For settling velocity, the particle velocity relative to the fluid is sought, which requires an estimate of the fluid velocity relative to the image frame. A common application of PIV methods is to estimate fluid velocities from the motions of suspended particles sufficiently small to approximate fluid motions. In the present application, PIV will be applied to digitally filtered image sequences including only small particles to estimate space- and time-variant fluid velocity fields through which the larger particles settle.

Small-particle selection

PIV tracer particles must be sufficiently small in size, mass, and settling velocity to closely approximate fluid motions. Ideal PIV tracer particles are smaller than the scale of fluid motion to be measured, capable of scattering sufficient light to be detected by the imaging device, and neutrally buoyant (Westerweel 1993; Raffel et al. 2007). Within video settling columns, we rely on natural tracer particles and the tracer characteristics cannot be tailored to meet experimental requirements. Instead, the natural tracers will be evaluated to estimate the particle size range that meets the application requirements related to frequency response and settling bias.

Frequency response of small particles in accelerating flows is influenced by the excess particle density and drag. The Stokes response time, $\tau_s = d^2\rho_p/(18\mu)$, is commonly used to evaluate the frequency response of potential PIV tracer particles (Bec et al. 2006; Raffel et al. 2007), where d is particle diameter, ρ_p is particle density, and μ is fluid dynamic viscosity (0.0018–0.0008 $\mathrm{kg{\cdot}m^{-2}{\cdot}s^{-1}}$ for water between 0°C and 30°C). For τ_s much less than the time scales of interest, the tracer particles are considered to appropriately follow fluid

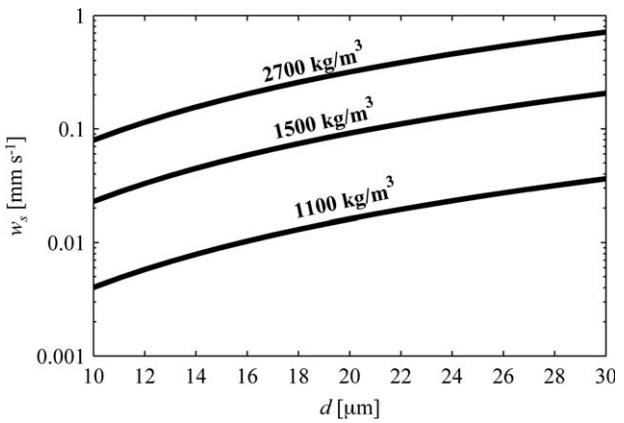

Fig. 3. Stokes settling velocity estimate for candidate small-particle diameters and densities.

velocities, with near-equal amplitude and phase (Hjelmfelt and Mockros 1966). For video settling columns, the small particles to be tracked by PIV methods are individual silt-sized mineral grains ($\rho_p \approx 2700$ kg·m^{-3}) or microflocs composed of clay, silt, and organic matter ($1020 < \rho_p < 1500$ kg·m^{-3}). Evaluating the limiting case for 30 μm mineral particles, the estimated Stokes response time is 10^{-4} s, much smaller than the 0.5- to 2-s time scales of fluid motion within the settling column.

Because the natural tracers are generally not neutrally buoyant, settling of the tracer particles introduces some degree of bias in the vertical component of the estimated fluid velocities. Stokes settling, $w_s = \left(\rho_p - \rho_w\right) g d^2/(18\mu)$ describes the settling velocity of spherical particles at small-particle Reynolds number ($Re_p = w_s d/\nu \ll 1$), where ρ_w is fluid density, g is gravitational acceleration, and ν is fluid kinematic viscosity. Stokes settling velocity was estimated for particles ranging in diameter and density from 10 μm to 30 μm and 1100–2700 kg m^{-3} (Fig. 3). For the case in which much of the suspended material is aggregated (and has lower density), the 10–20 μm size range has an estimated settling bias between 4×10^{-3} mm·s^{-1} and 1×10^{-1} mm·s^{-1}. Numerous studies suggest that in natural muddy environments few suspended particles in the 10–20 μm size range are completely disaggregated (Krank and Milligan 1992; Mikkelsen and Pejrup 2000; Droppo 2004; Smith and Friedrichs 2011) with particle densities equal to mineral density (2700 kg·m^{-3}). Therefore, in most cases, the settling bias is likely to be within the lower portion of the stated range, i.e., $\leq \sim 0.1$ mm s^{-1}. Choosing particles smaller than 15 μm will reduce the settling bias, but the gains in doing so are largely offset by the lower light scattering potential and practical limits of resolving such particles with the present optics. Nonetheless, it should be recognized that if one applies this method in environments where completely disaggregated mineral grains are abundant in the medium silt size range, mean biases are likely to be larger.

Image processing

The initial step of the PIV analysis includes image preprocessing to remove background illumination, conversion of grayscale images to binary, and region property estimates of the binary image as described for PTV. The resulting binary image is filtered to remove particles with sizes exceeding the small-particle criterion. To provide equal weighting of the small particles during cross-correlation, each small binary particle is replaced with a 3×3 binary representation. The 3×3 representation was implemented to allow some spatial jitter in the frame-to-frame cross-correlation, which was found through experimentation to provide more stable peaks in the cross-correlation than alternate methods. Raffel et al. (2007) summarize alternate methods for correlation signal enhancement with variable particle image intensity.

The PIV method involves binning the image into subregions or interrogation areas. For the present application, the 1380×1024 image frame was subdivided into 10×8 interrogation areas with corresponding pixel dimensions of 136

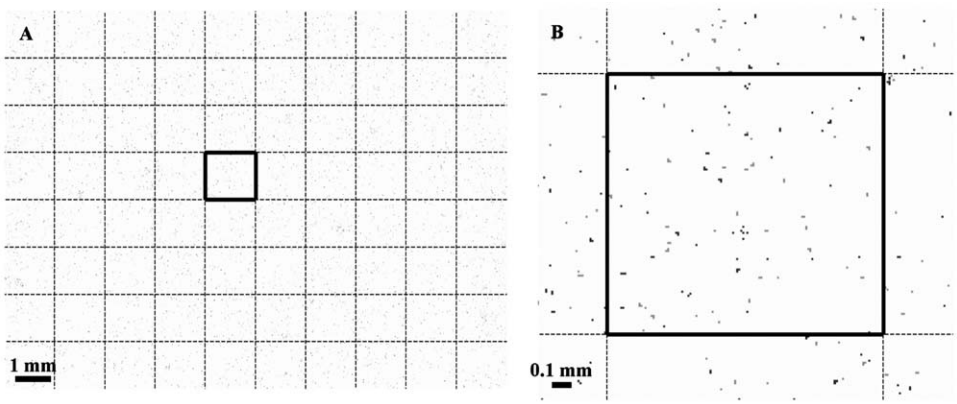

Fig. 4. (A) Image with interrogation areas (1.4 mm $\times$ 1.3 mm) for PIV analysis. (B) A single interrogation area (from the bold box in (A)) indicating small particles from two temporally adjacent frames. The lighter-shaded particles are from frame *I* and the darker-shaded particles are from frame *I*+1.

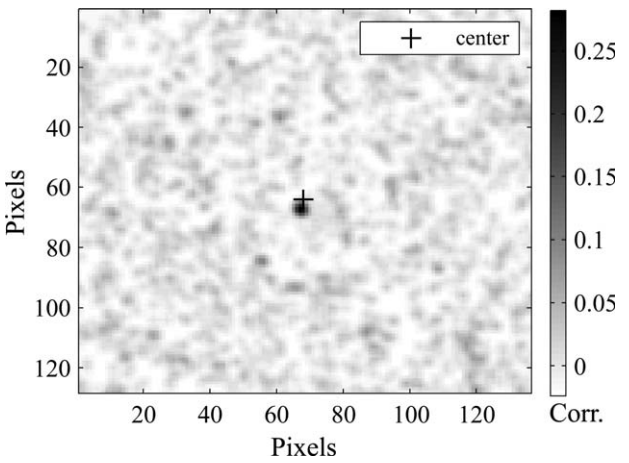

Fig. 5. Cross-correlation matrix for interrogation area from Fig. 4. The peak determines the displacement vector of small particles between frames.

× 128 and spatial dimensions of approximately 1.4 × 1.3 mm. An example image with defined interrogation areas is presented in Fig. 4a. The inset in Fig. 4b shows small particles within a single interrogation area. The darker-shaded small particles are from frame *I* and the lighter-shaded particles are from frame *I*+1. The interrogation area from frame *I* is cross-correlated to a larger interrogation area in frame *I*+1. The frame *I*+*1* interrogation area is twice the size of and centered on the frame *I* interrogation area. The resulting cross-correlation for the inset interrogation area from Fig. 4 is presented in Fig. 5.

The peak correlation in Fig. 5 defines the displacement of the small particles between frames *I* and *I*+1. The relatively weak peak correlation in Fig. 5 is related to the relatively poor signal-to-noise ratio for the small PIV particles. One of the challenges of this application is to sufficiently light the small PIV particles without oversaturating the larger PTV particles. Defining the correlation peak in this discrete fashion (based on the pixel location of the peak correlation) limits the PIV velocity resolution to 1 pixel/frame interval. For the typical application of PICS, this limit is approximately 10 μm/0.1 s, i.e., 0.1 mm s^{-1}. While this can be considered sufficient for the present application, sub-pixel resolution of particle displacements is possible through peak-fit estimators to a resolution of better than 0.1 pixel displacement (Westerweel 1993; Raffel et al. 2007). Implementing a peak-fit estimator to the PIV would then increase the velocity resolution for the PICS to the order of 0.01 mm s^{-1}.

The final step in PIV analysis involves detection and replacement of spurious vectors. Spurious vectors result from peak correlations between the kernel and target interrogation areas away from the true displacement vector and generally result from small numbers of tracer particles within the interrogation area. Some spurious vectors are readily apparent to the eye as shown in the upper right interrogation area of Fig. 6a. (The red arrows in Fig. 6a also highlight all interrogation areas with fewer than five PIV particles.) Research in digital PIV methods has lead to efficient algorithms for detection and replacement of spurious vectors. The normalized median test (Westerweel 1994; Westerweel and Scarano 2005) is a robust and computationally efficient method for detecting spurious vectors. The normalized median test detects spurious vectors by identifying large local deviations in velocity field compared to neighboring interrogation areas. A particular strength of the normalized median test is that a single detection threshold may be developed and applied to a wide range of flow conditions for a particular application. For the present application, the user is required to adjust the detection threshold until all spurious vectors are detected. (The threshold in this example was set to 2, the value recommended by Westerweel and Scarano (2005).) The experimentally determined threshold can then be applied generally for a set of settling experiments.

Replacement of spurious vectors is accomplished through a two-step process in the spatial and temporal domains. In the spatial domain, spurious vectors detected with the

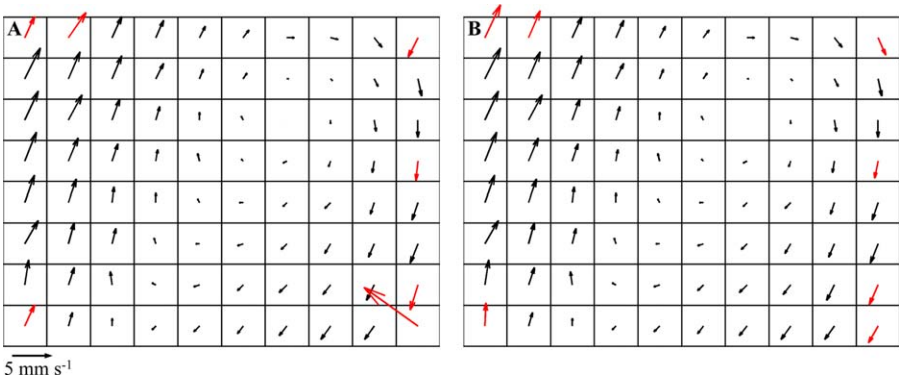

Fig. 6. PIV determined velocity vectors. Boxes indicate interrogation areas (1.4 mm × 1.3 mm) (A) vectors resulting from the PIV cross-correlation, including spurious vectors (red). (B) vectors following spurious vector detection and replacement (replaced vectors indicated in red). Maximum velocity in (B) is 1.5 mm s^{-1}.

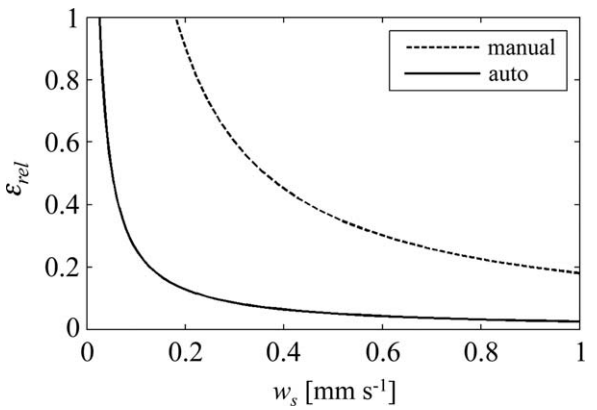

Fig. 7. Relative error ($\varepsilon_{rel} = |\delta w_s/w_s|$) in settling velocity estimate for manual method (Smith and Friedrichs 2011) and automated PIV method.

normalized median test are replaced with an inpainting method. Digital inpainting is a method developed for image restoration for which corrupted portions of an image are smoothly filled based on the neighboring valid portions of the image. The numerical basis for the inpainting method applied here is numerical solution of the Laplacian, $\nabla^2\mathbf{U} = 0$, for detected spurious vectors. This approach is particularly well suited for fluid dynamics applications as it follows potential flow theory—albeit in only two dimensions. The code implemented in the PICS image analysis software is INPAINT_NANS, authored by John D'Errico. The spatially replaced spurious vectors are then analyzed for outliers in the time domain via low-pass filtering and outlier detection, and are replaced by linear interpolation. In Fig. 6b, the seven spurious vectors of Fig. 6a have been detected and replaced.

Fluid-referenced settling velocities

The PTV velocities of large particles and the PIV velocities of small particles (which approximate fluid motions within the image plane) are used to estimate relative motions of the large particles to the surrounding fluid. The relative motion of the large particles to the surrounding fluid is given by:

$$\mathbf{V}_r(t) = \mathbf{V}(\vec{x}\,, t) - \mathbf{u}(\vec{x}\,, t) \tag{1}$$

where, $\boldsymbol{V}_r$ is the time-dependent velocity of the particle relative to the fluid, $\boldsymbol{V}$ is the space- and time-dependent velocity of the particle (in the fixed reference frame relative to the camera), $\boldsymbol{u}$ is the space- and time-dependent fluid velocity (also in the fixed reference frame), and $\vec{x} = x\hat{i} + z\hat{k}$ is 2-D spatial position. The fluid velocity components, u_x and u_z, are estimated by bilinear interpolation from the PIV velocity field at each PTV particle centroid throughout the image sequence. (The velocity field is extended to the image boundaries with the inpainting method described in Section 2.2.) The settling velocity (vertical component of the particle velocity relative to the fluid) is then defined as:

$$w_s = \frac{\Delta z}{\Delta t} - w_f \tag{2}$$

where Δz is vertical displacement of the particle centroid, Δt is the elapsed time over which the particle was tracked, and w_f is the vertical fluid velocity component.

Assessment

Evaluation of the PIV/PTV image analysis methods was performed to characterize measurement uncertainty and to quantify improvements gained over the procedure described in Smith and Friedrichs (2011).

Measurement uncertainty

Measurements with video-based methods for estimating particle size, settling velocity, and particle density are subject to measurement uncertainties. Smith and Friedrichs (2011) evaluated uncertainties for the PICS associated with particle size and the manual tracking of 10 small particles to determine a mean fluid velocity. This section assesses measurement uncertainty of the automated PIV-based fluid velocity estimates, following the approach presented in Smith and Friedrichs (2011).

Settling velocity

Estimated settling velocity (Eq. 2) depends on measured particle translation, elapsed time over which each particle was successfully tracked, and estimated vertical fluid velocity. Uncertainties associated with each of the measured parameters contribute to the settling velocity uncertainty as:

$$\delta w_s = \sqrt{\left(\frac{\partial w_s}{\partial(\Delta z)}\delta(\Delta z)\right)^2 + \left(\frac{\partial w_s}{\partial(\Delta t)}\delta(\Delta t)\right)^2 + \left(\frac{\partial w_s}{\partial(w_f)}\delta(w_f)\right)^2} \tag{3}$$

assuming independent and random measurement uncertainties (Taylor 1997). Within this expression, δ indicates the measurement uncertainty for the given parameter and partial derivatives were determined from Eq. 2. Parameter uncertainties, $\delta(\Delta z)$ and $\delta(\Delta t)$, were determined experimentally (Smith and Friedrichs 2011) to be about 10^{-2} mm, and 10^{-5} s, respectively. Uncertainty in the PIV-estimated fluid velocity was determined from numerical experiments with a sinusoidal vertical velocity field with 2 mm s^{-1} amplitude and 4.3 s period. The simulated conditions represent flow conditions observed within PICS while suspended in the water column, tethered to a small vessel in rough chop. Randomly placed small particles (with zero settling velocity) were transported within this velocity field, converted to digital video, and tracked by the PIV software. The PIV-estimated velocities were then compared to the prescribed velocities, resulting in an RMS error, $\delta(w_f)$, of 0.025 mm s^{-1}.

Applying the determined parameter uncertainties to Eq. 3 gives an uncertainty in w_s equal to 0.026 mm s^{-1}. The PIV-estimated fluid velocity is the largest contributor of random uncertainty at 96%, followed by the particle positioning

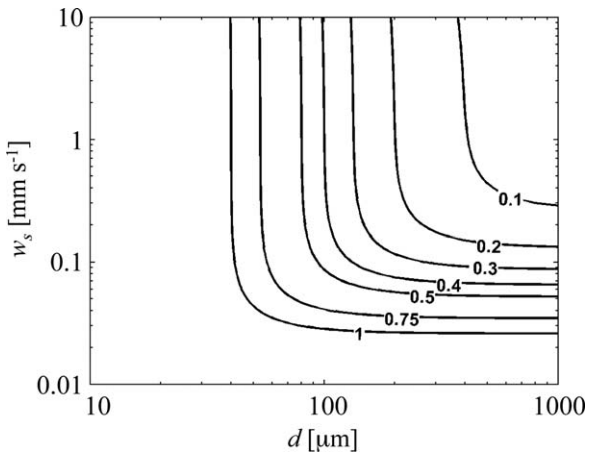

Fig. 8. Contours of excess density relative error ($\varepsilon_{rel} = |\delta\rho_e/\rho_e|$) for automated PIV method.

uncertainty (4%), and the negligibly small timing uncertainty. Relative settling velocity uncertainties ($\delta w_s/w_s$) for the automated and manual PIV methods were determined by normalizing Eq. 3 with settling velocity (Fig. 7). The error parameters for Eq. 3 were determined from a combination of measured data and simulation. The automated PIV method significantly reduces (by factor of 7) the settling velocity measurement uncertainty over the manual fluid velocity method. Relative uncertainty levels of 0.1, 0.5, and 1 are associated with settling velocities of 0.26, 0.05, and 0.026 mm·s^{-1}, respectively. The difference in error between the manual fluid velocity model and the PIV method is unrelated to the number of large particles tracked. The key difference is between tracking a few small particles to determine one average fluid velocity for the whole field of view in the manual method—as suggested by Van Leussen and Cornelisse (1993)—vs. resolving the space and time-variant velocity field with the automated PIV method.

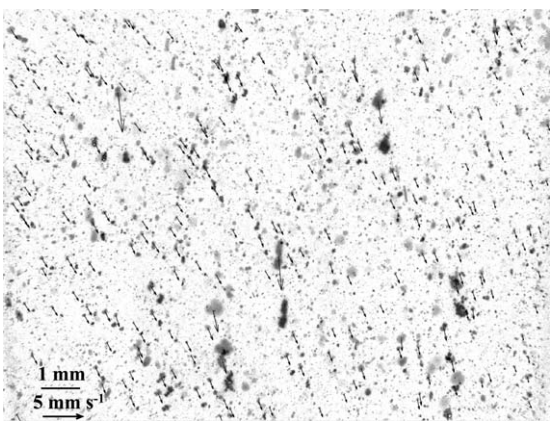

Fig. 9. Particle images and displacement vectors from PTV analysis. Particle displacements are indicated from two superimposed image frames (separated by 0.375 s). Particle images are negative representations of the raw images with logarithmic intensity scaling. Particle intensity from the first image is decreased by 25% to better indicate direction of motion. Vector lengths are scaled for display purposes and are not related to the length scale provided.

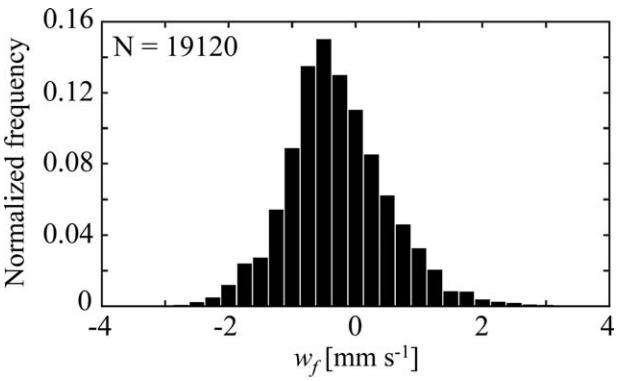

Fig. 10. Histogram of vertical fluid velocities from a single image sequence (240 frames). Mean vertical velocity is −0.305 mm s^{-1} (downward).

Excess density

Smith and Friedrichs (2011) rearranged Soulsby's (1997) empirical settling velocity expression to estimate excess particle density

$$\rho_e = \rho_p - \rho_w = \frac{\rho_w \nu^2}{g K_2 d^3}\left[\left(\frac{w_s d}{\nu} + K_1\right)^2 - K_1{}^2\right] \quad (4)$$

where ρ_p is particle density, ρ_w is water density, ν is kinematic viscosity, g is gravitational acceleration, d is particle diameter, $K_1 = 10.36$, and $K_2 = 1.049$. By Eq. 4, excess particle density is estimated from measurements of settling velocity, particle diameter, fluid density, and fluid viscosity. Assuming

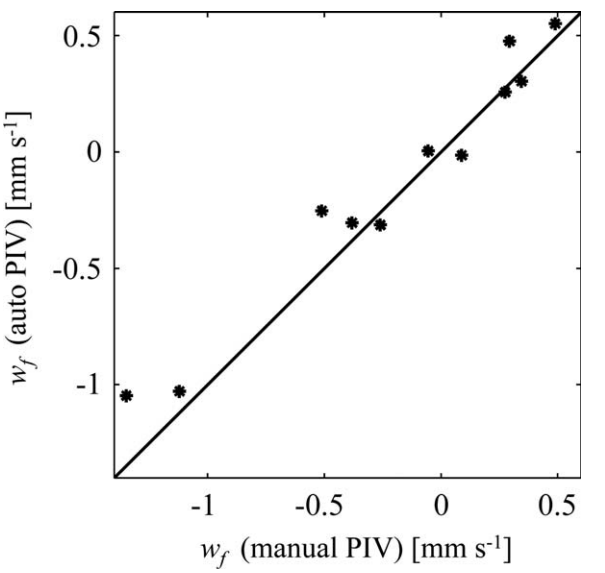

Fig. 11. Comparison of mean vertical fluid velocities determined from automatic PIV and manual PIV methods for 11 image sequences.

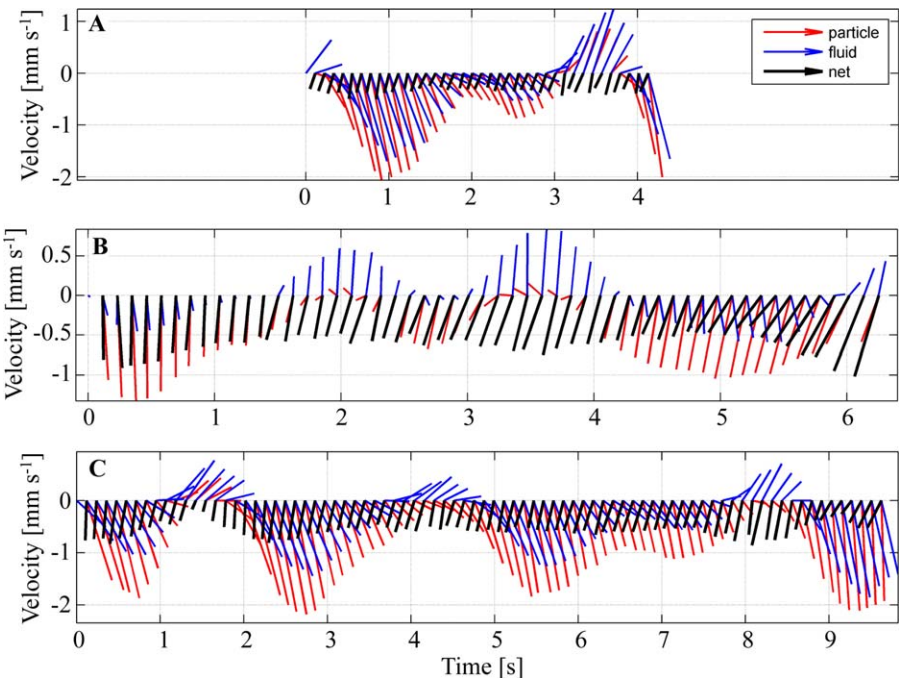

Fig. 12. Time-series velocities for three-tracked particles of size (A) 51, (B) 100, and (C) 200 μm. Vectors indicate particle velocity (red), local fluid velocity (blue), and net (settling) velocity (black).

uncertainties in fluid density and viscosity are small and uncertainties in settling velocity and particle size are independent and random, the uncertainty in excess density is given by:

$$\delta\rho_e = \sqrt{\left(\frac{\partial\rho_e}{\partial w_s}\delta w_s\right)^2 + \left(\frac{\partial\rho_e}{\partial d}\delta d\right)^2} \quad (5)$$

where the partial derivatives refer to terms in Eq. 4. The relative error in excess density (Fig. 8) was determined by applying the previously determined uncertainties, $\delta w_s = 0.026$ mm·s^{-1} and $\delta d = 0.02$ mm (Smith and Friedrichs 2011) and normalizing the result ($\delta\rho_e/\rho_e$). The largest uncertainties are associated with small, slowly settling particles. For macroflocs ($d > 150$ μm) settling faster than 0.1 mm·s^{-1} relative error in excess density is < 0.35.

Application to field data

To demonstrate the PTV and PIV methods for automated particle tracking, they are applied here to a single settling velocity video (of 33 total) collected within a clamshell dredging plume in Boston Harbor on 11 September 2008. The dredged bed material at the site was characterized as 54% sand, 37% silt, and 9% clay. The PICS water sample was collected and image acquisition performed approximately 60 m down current from the dredging source at a depth of 10 m below the water surface. Image acquisition began approximately 20–40 s following collection of the PICS water sample, and images were recorded at eight frames per second for 30 s (240 frames). In the following sections, the results and performance of the PTV and PIV are examined and compared to alternate image processing methods.

PTV particle tracking

PTV processing was performed on the image sequence. Background illumination for each pixel was defined as the modal illumination level (typically 1/255 to 2/255) for that pixel as sampled randomly in time from 50 frames. Grayscale thresholding was determined by the automatic thresholding method of Lintern and Sills (2006), resulting in a grayscale threshold of 13/255, and the minimum particle size for PTV tracking was set to 30 μm. For the 240 image frames, 2785 particles were tracked with thread lengths greater than four frames (0.5 s). Particles ranged in size from 32 μm to 550 μm, with vertical velocities (positive upward) ranging from -9.9 mm s^{-1} to 4.6 mm s^{-1}, and thread lengths from 4 frames to 145 frames.

An example of particle image pairs and PTV-estimated particle velocities is presented in Fig. 9. To more clearly indicate particle displacements, particles are shown from frames I and $I+3$, resulting in a frame interval of 0.375 s. All imaged particles (including those not resulting in a particle thread) are shown, and image intensities are displayed with a logarithmic scale to effectively visualize the large, bright particles and smaller, dimly illuminated particles. The velocity vectors for displacements between frames I and $I+1$ are positioned on the tracked particles from frame I. In Fig. 9, the influence of fluid motions on the settling particles is evident by

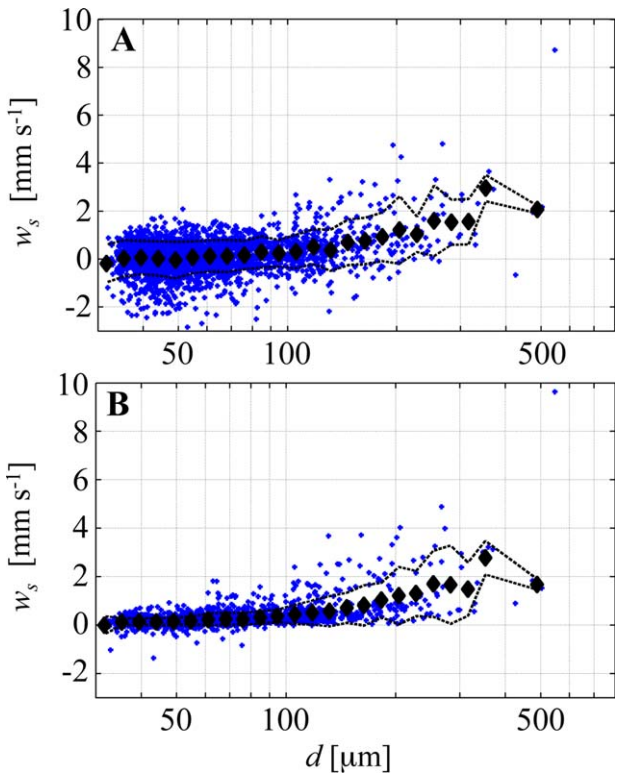

Fig. 13. Settling velocity vs. particle diameter. (A) corrected with mean vertical velocity estimated from 10 manually tracked small particles, (B) corrected with fluid velocities estimated by PIV method. $N = 2785$ tracked particles, filled diamonds indicate bin-averaged velocities for bins with three or more particles, dashed lines indicate +/− 1 SD.

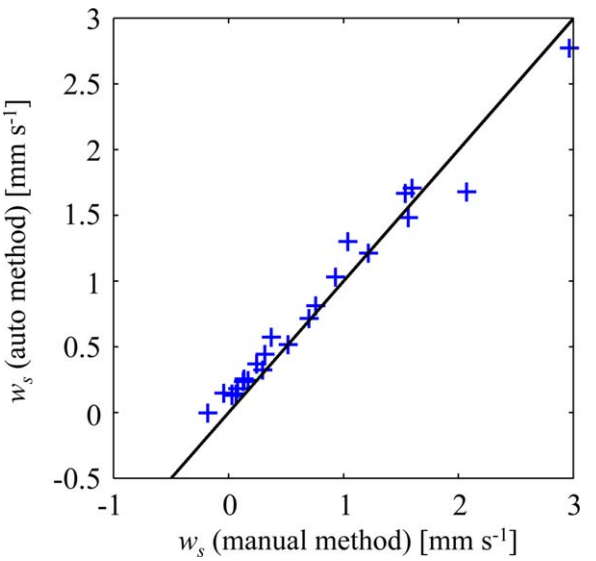

Fig. 14. Comparison of bin-averaged settling velocities with manual and automatic PIV methods for particle tracking data from Fig. 13.

comparing the directions of the more slowly settling particles to the faster-settling particles, which reinforces the requirement to adjust particle settling velocities with estimates of fluid motion.

PIV fluid velocity estimates

PIV analysis was performed on the small particles in the image sequence to estimate fluid velocities within the image plane. The background illumination determined during the PTV analysis was subtracted from all image frames, followed by grayscale to binary conversion with a manually prescribed threshold of 4/255 (to better define the fainter small particles). Only binary particles smaller than 21 μm were retained for the PIV analysis. The PIV interrogation areas for frame I were established as a 10 × 8 grid (136 × 128 pixels or 1.46 × 1.37 mm) with the frame $I+1$ interrogation area twice the size of and centered on the frame I interrogation area. Spurious vectors were detected with the normalized median test (Westerweel and Scarano 2005) on a 3 × 3 interrogation area neighborhood without boundary buffering. Spurious vector replacement in the space- and time-domains was performed as described in Materials and Procedures section. The PIV analysis results in 19,200 velocity vectors of which 1392 (7%) were detected and replaced as spurious. The mean vertical fluid velocity estimated from the PIV analysis was −0.30 mm s^{-1} (downward) with a probability distribution as shown in Fig. 10. The negative (downward) mean fluid velocity in this example represents the average fluid motion within the central portion of the settling column cross-section. Mean fluid velocities at the imaging plane were both positive and negative during this field experiment (see Fig. 11).

Manual tracking of small particles using the method described by Smith and Friedrichs (2011) was performed on the example image sequence. By this method, 10 small particles (uniformly distributed in space and time) are selected and tracked manually to determine the mean vertical fluid motions. The manual tracking method results in a mean vertical fluid velocity of −0.38 mm s^{-1} (compared to −0.30 mm s^{-1} by the automated PIV method). Additionally, mean vertical fluid velocities were estimated by the manual tracking method for 11 of the image sequences collected from the Boston Harbor field experiment and compared to the automated PIV method (Fig. 11). The comparison reveals that the manual method results in a reasonably accurate mean fluid velocity from a small sample of particle velocities. Most results of the manual method are within 0.1 mm s^{-1} of the automated method, but a few experiments are in error by as much as 0.2–0.3 mm s^{-1}. The larger of these differences are relatively large compared to the settling velocities of interest (on the order of 0.1–0.5 mm s^{-1}).

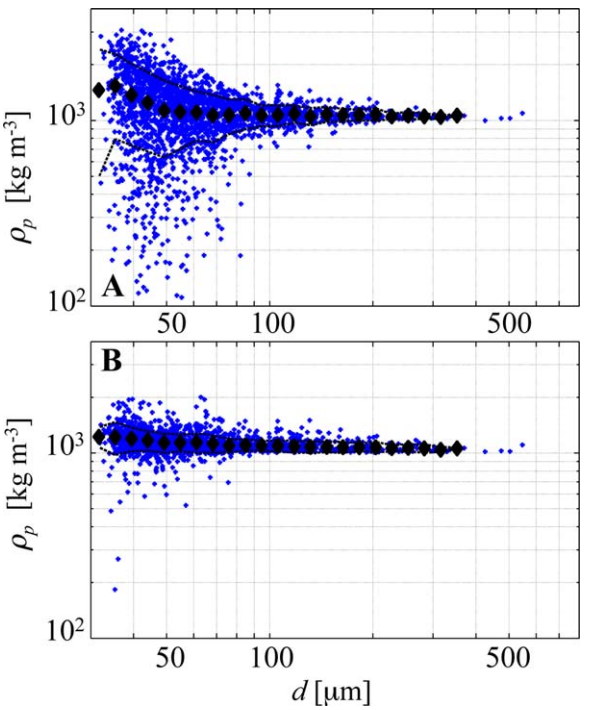

Fig. 15. Particle density vs. particle diameter. (A) corrected with mean vertical velocity estimated from 10 manually tracked small particles, (B) corrected with fluid velocities estimated by PIV method. $N = 2785$ tracked particles, filled diamonds indicate bin-averaged densities for bins with three or more particles, dashed lines indicate +/− 1 SD.

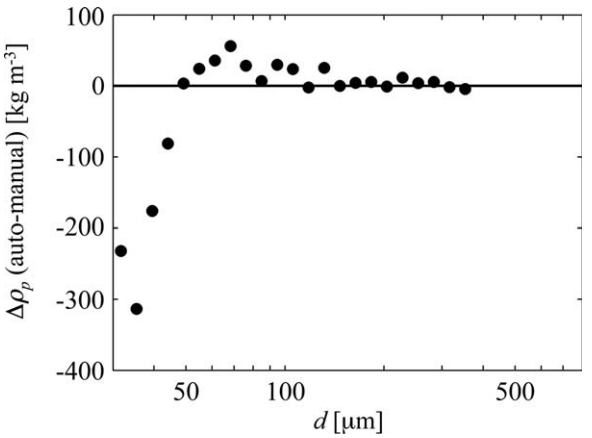

Fig. 16. Difference between bin-averaged (by size) particle densities between manual and automatic PIV methods for particle tracking data from Fig. 15.

Settling velocity

Settling velocities of flocs and bed aggregates (the larger particles) are corrected with the spatially and temporally variant fluid velocities estimated from the PIV analysis. Three individual particle threads from the PTV analysis are selected to illustrate the PIV corrections to PTV velocities to result in fluid-relative settling velocities. Figure 12 provides PTV particle velocity, PIV fluid velocity, and net settling velocity for particles with diameters of 51, 100, and 200 μm. Each of these particles settled through a time- and space-variant velocity field. Vertical fluid oscillations were induced by vessel motions associated with wind waves and passing vessel wakes, resulting in peak vertical fluid velocities on the order of 1–2 mm·s^{-1}. Particle velocities largely follow the fluid velocities with a negative (downward) bias reflecting the particle settling velocity. Subtracting the fluid velocity from the particle velocity results in a near-constant settling velocity (net) of the particles relative to the fluid. Mean settling velocity for a given particle thread is then defined as the vector average of the net velocity.

Improvements gained through automated PIV determination of time- and space-variant fluid velocities are quite apparent in comparing the settling velocity estimates for all tracked particles (Fig. 13). In Fig. 13a, PTV particle velocities were corrected with the mean vertical fluid velocity estimated by the manual method (manually tracking 10 small particles); Fig. 13b provides the settling velocities corrected with PIV-estimated fluid velocities for the same image sequence. The automated PIV method effectively reduces the apparent variance in settling velocity by accounting for the variance in vertical fluid velocity, especially for particles less than 100 μm in diameter. The bin-averaged standard deviation for w_s (± 1 SE) for $d < 100$ μm in Fig. 13 is 0.68 ± 0.02 mm s^{-1} for the manual method but only 0.21 ± 0.02 mm s^{-1} for the automated method. The bin-averaged (by particle size) settling velocities between the two methods are generally consistent, especially for the larger, faster-settling particles (for $d > 100$ μm, the mean of the bin-averaged w_s values in Fig. 13 is 1.20 ± 0.21 mm s^{-1} for the manual case and 1.22 ± 0.18 mm s^{-1} for the automated case). Figure 14 presents a direct comparison of the bin-averaged settling velocities between the two methods. The negative bias of the manual method relative to the automated method is attributed to the larger estimate of mean fluid velocity (-0.38 ± 0.24 mm s^{-1} vs. -0.305 ± 0.006 mm s^{-1}) by the manual method. Otherwise, the bin-averaged settling velocities determined with the manual method are comparable to the automated PIV method.

Particle density

A further benefit of the automated PIV method is more accurate estimation of individual particle densities from the combined particle size and settling velocity information (Fig. 15). Particle densities were estimated using settling velocities corrected with the manual method (Fig. 15a) and the automated PIV method (Fig. 15b). As seen with settling velocity, the automated PIV method analogously reduces the spread in particle density by accounting for spatial and temporal variation in the vertical fluid velocity. Variations

in manual and PIV estimates of particle density are similar for particle sizes larger than 200 μm, but the manual method results in significantly greater variance (by a factor of 2–5) for particle sizes smaller than 100 μm. The bin-averaged standard deviation for ρ_p ($\pm$ 1 SE) for $d < 100$ μm in Fig. 15 is 457 ± 77 kg m^{-3} for the manual method but only 133 ± 15 kg m^{-3} for the automated method. Differences between the automatic-PIV and manual-method estimates of particle density (bin-averages) are presented in Fig. 16. The differences are small for particles larger than 100 μm. For particle diameters between 50 μm and 100 μm, density differences between 10 kg·m^{-3} and 60 kg·m^{-3} are attributed to differences in estimated bin-averaged settling velocity (Fig. 14). The manual correction method estimates larger densities for particle diameters < 50 μm, which is a data processing artifact associated with exclusion of negative densities from the analysis.

Computational requirements

Fully automated PTV and PIV image analysis greatly reduces the time required to analyze video settling column images compared to manual or semiautomated analysis. The following discussion defines the computational effort required for the automated methods with presently available computing hardware. The automated analysis presented herein was performed on a system with dual 2.66 GHz Intel® Xeon® E5430 quad-core processors and 3 GB of RAM. The PIV and PTV analyses were written and executed in Matlab®, utilizing the Image Processing Toolbox™ for most image processing functions.

Computational requirements for PTV analysis depend on the number, size, and settling velocity of tracked particles and number of frames in the video. Most of the computational load is associated with the normalized image cross-correlations performed during the particle matching process. The computational load for this process is dependent on the number of matches required and the size of the kernel and target images. Wall clock times to complete PTV analysis on a 1380 $\times$ 1024 video with 240 frames range between 2 min and 20 min. Time required to track 1000 particles over 240 frames is generally 5–8 min.

Computational requirements for PIV analysis are dependent on image size, number of frames, and subdivision level. Similar to PTV analysis, most of the computational load is associated with the kernel-template matching with normalized image cross-correlation. PIV analysis on 1380 $\times$ 1024 video with 240 frames and 10 $\times$ 8 image subdivision took approximately 50 min to complete. Potential approaches for reducing computation time include recoding in Fortran or C and/or code parallelization.

Manual processing is labor-intensive, requiring the user to match particles between adjacent frames, determine particle size, and estimate settling velocity. Semiautomated processing routines (for which the user determines particle matching and image processing routines determine particle size and settling velocity) reduce processing time but still demand substantial human resources compared to fully automated methods. Semiautomated PTV analysis takes approximately 1–2 min per particle, and fluid velocity estimates require another 2–3 min per particle. By these estimates, tracking 1000 particles in a 240-frame image sequence would require approximately 50–80 h of human interaction, compared to less than one minute of human interaction and one hour of computer time for the fully automated PTV/PIV method presented here.

Application requirements and limitations

The application of PTV and PIV to video settling column images imposes several requirements on the imaging system. Adrian (1991), Raffel et al (2007), and Steinbuck et al. 2010 provide general overviews of PIV and PTV imaging requirements and limitations. We will highlight a few of the key requirements, specific to the methods described previously for video settling column image analysis. The video imaging system design should address several key requirements including: imaging geometry, magnification, resolution, light intensity, strobe duration, and frame rate. Due to the imaging geometry, multiple points in the "world coordinate" unavoidably map to a single point in the image plane, introducing perspective-based sizing errors and potentially overlapping particle silhouettes. This can be minimized through a combination of a narrow depth of field (relative to the focal length) and a thin light sheet. If the field is too narrow, however, particles may leave the field too quickly.

The acquired images should have sufficient magnification to resolve the largest of the small PIV tracer particles with 2–4 pixels (to ensure a sufficient number of PIV particles larger than one pixel). At high magnification (near 1 : 1), lens quality becomes more important and balancing depth-of-field and diffraction limits becomes more challenging. Increasing magnification also reduces the field of view (sample size). Sample size reduction is undesirable for imaging of macroflocs, which generally occur in low abundance but often contribute a large proportion of suspended sediment mass and vertical mass flux. Image size and magnification should be balanced such that the small PIV tracers are sufficiently resolved while maximizing the sample volume to increase numbers of particles for PTV particle tracking and analysis. Magnification and frame rate also influences the maximum resolvable particle velocities by PTV. Frame rate should be sufficiently fast to capture approximately five-particle images for the fastest settling particles (a requirement for rejection of spurious PTV velocities).

Light intensity and contrast are key elements for the combined PIV and PTV analysis of settling velocity. The imaging sensor must receive sufficient reflected light from a wide

range of particle sizes in suspension with sufficient contrast to discern these particles from reflected and scattered light within the settling column. The small PIV tracer particles represent a particular challenge, given their low-intensity reflections. Factors influencing light intensity registered by the image sensor include: lighting intensity, lens size, vignetting, light reflection by viewing ports and lens elements, extension tubes, image sensor fill factor, and quantum efficiency. Use of high-intensity and focused lighting, lenses with antireflective coatings, and high-sensitivity, low-noise image sensors addresses many of these issues. Contrast between the imaged particles and surrounding fluid can be improved by reducing internal reflections and light scattering surfaces within the settling column. Additionally, the dynamic range (bit depth) of recorded images should be fully utilized through adjustment of the lighting source or camera gain, keeping in mind that camera gain also amplifies sensor noise.

Light scattering and particle obscuration increase with increasing suspended sediment concentration. The smaller and less bright PIV tracer particles are impacted at lower mass concentrations than larger PTV-tracked particles. Concentrations at which PIV and PTV analysis are impacted are dependent on particulate size and optical path length. Experience with the PICS (4.5 cm light path, 2 cm imaging distance) suggests that suspended sediment concentrations between 50 mg L^{-1} (for disaggregated fine silt) and 300 mg L^{-1} for well-aggregated suspensions begin to impact image analysis.

Discussion

Fluid motions within video settling columns have been a persistent challenge that in many cases limits the experimental potential of such devices. Researchers (Van Leussen and Cornelisse 1993; Fennessy et al. 1994) have used physical measures such as separate capture and settling chambers, reductions in thermal input, and introduction of density gradients to damp turbulence and reduce fluid motions. Additionally, efforts have been made to quantify fluid motions by manually tracking small particles (Van Leussen and Cornelisse 1993; Smith and Friedrichs 2011). An automated method to define spatial and temporal variations in fluid motions is presented and evaluated, by which the population of particles smaller than 20 μm is tracked by PIV to approximate fluid motions. Application of the PIV method to correct velocities of larger particles (tracked with PTV methods) permits accounting for time- and space-variant fluid velocities within the settling column and results in more accurate settling velocities and densities for the tracked larger particles ($>$ 30 μm in diameter). The bin-averaged (by size) settling velocities and densities determined by the manual and automated PIV methods were generally similar; however, estimates of settling velocity and density for individual particles were greatly improved by use of the automated method, and mean biases associated with manual evaluation of individual video samples were also reduced.

Automated particle tracking and fluid velocity estimates offer several advantages, both experimentally and during postexperimental analysis. Fluid velocity corrections during image analysis permits faster sampling during field experiments, through use of a single sampling and settling chamber. The single-chamber design of video settling devices allows rapid profiling of the water column with image sequences recorded on the order of 2-min intervals instead of 10–40 min intervals with two-chambered devices. Automated PTV tracking of large particles and PIV estimates of fluid velocities enables tracking of large numbers of particles, which provides better statistical characterization of size, settling velocity, and density of suspended particle populations. The automated PIV fluid velocity correction method significantly reduces measurement uncertainty in both settling velocity and inferred particle density.

Comments and recommendations

The methods presented here are not limited to sediment particles settling through water. The methods could also be applied to biological particles (eggs, larvae, plankton, pollen) settling in air or water. Recently, the methods presented in this article were applied to determine the size and settling velocities of winter flounder (*Pseudopleuronectes americanus*) eggs in seawater (Lackey et al. 2010).

Correcting PTV-estimated large-particle velocities with PIV-estimated fluid velocities resulted in improved estimates of the still-water settling velocity of cohesive sediment aggregates. Future enhancements to the PIV method should include sub-pixel displacement resolution and evaluation of alternate cross-correlation peaks and Kalman filtering during spurious vector replacement. For laboratory experiments, PIV tracer particles that are neutrally buoyant or have known settling velocities may be introduced to reduce the settling bias associated with experiments conducted in the natural setting. It is recommended that future laboratory experiments utilize monodisperse particles of known density in the size range of natural flocs to test the effects of 2-D imaging, particle rotation, and diffraction on estimating the diameter of three-dimensional particles.

References

Adrian, R. J. 1991. Particle-imaging techniques for experimental fluid mechanics. Annu. Rev. Fluid Mech. **23**: 261–304. doi:10.1146/annurev.fl.23.010191.001401

Agrawal, Y. C., and H. C. Pottsmith. 2000. Instruments for particle size and settling velocity observations in sediment transport. Mar. Geol. **168**: 89–114. doi:10.1016/S0025-3227(00)00044-X

Ayukai, T., and E. Wolanski. 1997. Importance of biologically mediated removal of fine sediments from the Fly River plume, Papua New Guinea. Estuar. Coast. Shelf Sci. **44**: 629–639. doi:10.1006/ecss.1996.0172

Bec, J., and others. 2006. Acceleration statistics of heavy particles in turbulence. J. Fluid Mech. **500**: 349–358. doi:10.1017/S002211200500844X

Cartwright, G. M., C. T. Friedrichs, and S. J. Smith. 2013. A test of the ADV-based Reynolds flux method for in situ estimation of sediment settling velocity in a muddy estuary. GeoMar. Lett. **33**: 477–484. doi:10.1007/s00367-013-0340-4

Cornelisse, J. M. 1996. The field pipette withdrawal tube (FIPIWITU). J. Sea Res. **36**: 37–39. doi:10.1016/S1385-1101(96)90768-6

Cowen, E. A., and S. G. Monismith. 1997. A hybrid digital particle tracking velocimetry technique. Exp. Fluids **22**: 199–211. doi:10.1007/s003480050038

Droppo, I. G. 2004. Structural controls on floc strength and transport. Can. J. Civ. Eng. **31**: 569–578. doi:10.1139/l04-015

Dyer, K. R., and others. 1996. A comparison of in situ techniques for estuarine floc settling velocity measurements. J. Sea Res. **36**: 15–29. doi:10.1016/S1385-1101(96)90766-2

Eisma, D. 1986. Flocculation and de-flocculation of suspended matter in estuaries. Neth. J. Sea Res. **20**: 183–199. doi:10.1016/0077-7579(86)90041-4

Fennessy, M. J., and K. R. Dyer. 1996. Floc population characteristics measured with INSSEV during the Elbe estuary intercalibration experiment. J. Sea Res. **36**: 55–62. doi:10.1016/S1385-1101(96)90771-6

Fennessy, M. J., K. R. Dyer, and D. A. Huntley. 1994. INSSEV: An instrument to measure the size and settling velocity of flocs in situ. Mar. Geol. **117**: 107–117. doi:10.1016/0025-3227(94)90009-4

Fugate, D. C., and C. T. Friedrichs. 2002. Determining concentration and fall velocity of estuarine particle populations using ADV, OBS and LISST. Cont. Shelf Res. **22**: 1867–1886. doi:10.1016/S0278-4343(02)00043-2

Gibbs, R. J., and L. N. Konwar. 1983. Sampling of mineral flocs using Niskin bottles. Environ. Sci. Technol.: **17**: 374–375. doi:10.1021/es00112a014

Gonzalez, R. C., R. E. Woods, and S. L. Eddins. 2004. Digital image processing using Matlab. Pearson Prentice Hall.

Haralick, R. M., and L. G. Shapiro. 1992. Computer and robot vision, v. 2. Addison-Wesley.

Hill, P. S., T. G. Milligan, and W. R. Geyer. 2000. Controls on effective settling velocity of suspended sediment in the Eel River flood plume. Cont. Shelf Res. **20**: 2095–2111. doi:10.1016/S0278-4343(00)00064-9

Hjelmfelt, A. T., and L. F. Mockros. 1966. Motion of discrete particles in a turbulent fluid. Appl. Sci. Res. **16**: 149–161. doi:10.1007/BF00384062

Khalitov, D. A., and E. K. Longmire. 2002. Simultaneous two-phase PIV by two-parameter phase discrimination. Exp. Fluids **32**: 252–268. doi:10.1007/s003480100356

Kiker, K. T., and C. Pan. 2000. PIV technique for the simultaneous measurement of dilute two-phase flows. J. Fluids Eng. **122**: 811–818. doi:10.1115/1.1314864

Kineke, G. C., R. W. Sternberg, and R. Johnson. 1989. A new instrument for measuring settling velocities in situ. Mar. Geol. **90**: 149–158. doi:10.1016/0025-3227(89)90038-8

Krank, K., and T. G. Milligan. 1992. Characteristics of suspended particles at an 11-hour anchor station in San Francisco Bay, California. J. Geophys. Res. **97**: 11373–11382. doi:10.1029/92JC00950

Lackey, T. C., S. C. Kim, D. Clarke, and J. Smith. 2010. Transport and fate of winter flounder eggs near dredging operations. In Proceedings of Western Dredging Association Conference. San Juan, Puerto Rico, 6–9 June.

Lewis, J. P. 1995. Fast template matching. Vision Interface 95, p. 120–123. Canadian Image Processing and Pattern Recognition Society, Quebec City, Canada, May 15–19.

Lintern, G., and G. Sills. 2006. Techniques for automated measurement of floc properties. J. Sediment. Res. **76**: 1183–1195. doi:10.2110/jsr.2006.085

Manning, A. J., and K. R. Dyer. 1999. A laboratory examination of floc characteristics with regard to turbulent shearing. Mar. Geol. **160**: 147–170. doi:10.1016/S0025-3227(99)00013-4

Manning, A. J., and K. R. Dyer. 2002. The use of optics for the in situ determination of flocculated mud characteristics. J. Opt. A **4**: S71–S81. doi:10.1088/1464-4258/4/4/366

Mehta, A. J. 1989. On estuarine cohesive sediment suspension behavior. J. Geophys. Res. **94**: 14303–14314. doi:10.1029/JC094iC10p14303

Mikkelsen, O. A., T. G. Milligan, P. S. Hill, and D. Moffatt. 2004. INSSECT—an instrumented platform for investigating floc properties close to the seabed. Limnol. Oceanogr. Methods. **2**: 226–236. doi:10.4319/lom.2004.2.226

Mikkelsen, O. A., and M. Pejrup. 2000. In situ particle size spectra and density of particle aggregates in a dredging plume. Mar. Geol. **170**: 443–459. doi:10.1016/S0025-3227(00)00105-5

Milligan, T. G., and P. S. Hill. 1998. A laboratory assessment of the relative importance of turbulence, particle composition, and concentration in limiting maximal floc size and settling behaviour. J. Sea Res. **39**: 227–241. doi:10.1016/S1385-1101(97)00062-2

Oseen, C. 1927. Hydrodynamik, chapter 10. Akademische Verlagsgesellschaft.

Owen, M. J. 1976. Determination of the settling velocities of cohesive sands. Hydraulics Research Report No. IT161.

Raffel, M., C. E. Willert, S. T. Wereley, and J. Kompenhans. 2007. Particle image velocimetry, 2nd ed. Springer.

Sanford, L. P., and others. 2005. Variability of suspended particle concentrations, sizes, and settling velocities in the Chesapeake Bay turbidity maximum, p. 211–236. In I. G. Droppo, G. G. Leppard, S. N. Liss, and T. G. Milligan [eds.], Flocculation in natural and engineered environmental systems. CRC Press.

Santschi, P. H., A. B. Burd, J. F. Gaillard, and A. A. Lazarides. 2005. Transport of materials and chemicals by nanoscale colloids and micro- to macro-scale flocs in marine, freshwater, and engineered systems, p. 191–210. In I. G. Droppo, G. G. Leppard, S. N. Liss, and T. G. Milligan [eds.], Flocculation in natural and engineered environmental systems. CRC Press.

Schiller, L., and A. Naumann. 1933. Über die grundlegenden Berechnungen bei der Schwerkraftaufbereitung, Z. VDI, v. 77.

Smith, S. J., and C. T. Friedrichs. 2011. Size and settling velocities of cohesive flocs and suspended sediment aggregates in a trailing suction hopper dredge plume. Cont. Shelf Res. **10**: S50–S63. doi:10.1016/j.csr.2010.04.002

Soulsby, R. L. 1997. Dynamics of marine sands. Thomas Telford.

Steinbuck, J. V., and others. 2010. An autonomous open-ocean stereoscopic PIV profiler. J. Atmos. Ocean. Technol. **27**: 1362–1380. doi:10.1175/2010JTECHO694.1

Sternberg, R. W., A. Ogston, and R. Johnson. 1996. A video system for in situ measurement of size and settling velocity of suspended particulates. J. Sea Res. **36**: 127–130. doi:10.1016/S1385-1101(96)90782-0

Syvitski, J. P. M., and E. W. H. Hutton. 1996. In situ characteristics of suspended particles as determined by the floc camera assembly FCA. J. Sea Res. **36**: 131–142. doi:10.1016/S1385-1101(96)90783-2

Taylor, J. R. 1997. An introduction to error analysis, 2nd ed. University Science Books.

Tsai, C. H., S. Iacobellis, and W. Lick. 1987. Flocculation of fine-grained lake sediments due to a uniform shear stress. J. Great Lakes Res. **13**: 135–146. doi:10.1016/S0380-1330(87)71637-2

Van der Lee, W. T. B. 2000. Temporal variation of floc size and settling velocity in the Dollard estuary. Cont. Shelf Res. **20**: 1495–1511. doi:10.1016/S0278-4343(00)00034-0

Van Leussen, W. 1994. Estuarine macroflocs and their role in fine-grained sediment transport, ministry of transport, public works and water management. National Institute for Coastal and Marine Management (RIKZ).

Van Leussen, W., and J. M. Cornelisse. 1993. The determination of the sizes and settling velocities of estuarine flocs by an underwater video system. Neth. J. Sea Res. **31**: 231–241. doi:10.1016/0077-7579(93)90024-M

Voulgaris, G., and S. T. Meyers. 2004. Temporal variability of hydrodynamics, sediment concentration and sediment settling velocity in a tidal creek. Cont. Shelf Res. **24**: 1659–1683. doi:10.1016/j.csr.2004.05.006

Westerweel, J. 1993. Digital particle image velocimetry: Theory and application. Delft University Press.

Westerweel, J. 1994. Efficient detection of spurious vectors in particle image velocimetry data. Exp. Fluids **16**: 236–247. doi:10.1007/BF00206543

Westerweel, J., and F. Scarano. 2005. Universal outlier detection for PIV data. Exp. Fluids **39**: 1096–1100. doi:10.1007/s00348-005-0016-6

Williams, N. D., D. E. Walling, and G. J. L. Leeks. 2008. An analysis of the factors contributing to the settling potential of fine fluvial sediment. Hydrol. Processes **22**: 4153–4162. doi:10.1002/hyp.7015

Acknowledgments

The research presented in this article was conducted under the Dredging Operations and Environmental Research (DOER) program, Dredged Material Management Focus Area at the US Army Engineer Research and Development Center. DOER Program Manager is Dr. Todd Bridges. The manuscript was substantially improved by the insightful comments of Dr. Jules Jaffe and two anonymous reviewers. Additional support for Friedrichs's participation in this study was provided by the National Science Foundation Division of Ocean Sciences Grants OCE-0536572 and OCE-1061781. Permission to publish this article was granted by the Office, Chief of Engineers, US Army Corps of Engineers. This article is contribution No. 3204 of the Virginia Institute of Marine Science, College of William and Mary.

Submitted 24 June 2014
Revised 18 February 2015
Accepted 1 March 2015

Associate editor: Dr. Paul Kemp